

Supplementary Information

Ce⁴⁺ as a facile and versatile surface modification reagent for templated synthesis in electrical applications

Lulu Yao^a, Jiajun Gu^{*a}, Weiqiang Wang^a, Tengfei Li^a, Dongling Ma^{*b}, Qinglei Liu^a, Wang Zhang^a, Waseem Abbasa, Ashkan Bahadoran^a, and Di Zhang^a

^a State Key Laboratory of Metal Matrix Composites, Shanghai Jiao Tong University, Shanghai, 200240, China.

^b Énergie Mate´riaux Te´le´communications Research Centre, Institut National de la Recherche Scientifique, 1650 Boulevard Lionel-Boulet, Varennes, Que´bec, J3X 1S2, Canada.

*Correspondence to: gujiajun@sjtu.edu.cn; dongling.ma@emt.inrs.ca.

Table of content

1. Experimental procedures	3
1.1 Pretreatments of different substrates	3
1.2 Surface modification process of different substrates	3
1.3 Fabrication of various three-dimensional architectures	3
1.4 Material characterizations	4
1.5 Electrochemical test	5
2. Mechanism analysis of Ce⁴⁺ modification process	6
2.1 Characterization of modification process on other substrates	6
2.2 Morphology characterization of Ce-BFWs	8
2.3 Morphology characterization of other modified substrates	9
3. Mechanism analysis of growing three-dimensional architectures on substrates	11
3.1 Mechanism analysis of growing CeO ₂ on H ₂ O ₂ and HNO ₃ modified BFWs	11
3.2 Mechanism analysis of growing FeOOH on modified nickel foam	12
4. Morphology of three-dimensional architectures fabricated on unmodified and modified substrates	12
4.1 Morphology of CeO ₂ grown on unmodified substrates	12
4.2 Morphology of other 3D architecture fabricated on modified substrates.....	13
4.3 The XRD patterns of the nanomaterials on substrates	14
5. Electrocatalysis performance	15
5.1 Standardization of Hg/HgO referee electrode	15
5.2 Resistivity calculation of modified and unmodified nickel foam	16
5.3 Electrocatalysis performance of original nickel foam	16
5.4 Morphology comparison of FeOOH on nickel foam.....	17

1. Experimental procedures

1.1 Pretreatments of different substrates

Butterfly wings (BFWs) were immersed into ethyl alcohol for 10 min, and then washed three times with ethyl alcohol to remove the adsorbed impurities. The carbon paper (CP) and polyethylene terephthalate (PET) plank were first cleaned with ethyl alcohol in a sonic bath for 10 min, and then washed with distilled water for several times. The nickel foam (NF) was cleaned with ethyl alcohol and 6 wt.% HCl in a sonic bath for 10 min in order to remove the oxide on its surface. Then the NF was washed with distilled water for several times.

1.2 Surface modification process of different substrates

The surface modification process is same for all substrates. The only difference is the modification time, which depends on the intensity of the reaction between substrates and ceric ammonium nitrate (CAN). Firstly, the substrates were immersed into 0.1 M CAN aqueous solution under room temperature for certain time (5–15 min for BFWs; 20–30 min for CP, 15–30 min for NF and 2–4 h for PET). Then the modified substrates were washed with distilled water to get rid of redundant Ce^{4+} ions. Finally, the substrates were treated with 0.1 M NaOH aqueous solution for 1 min and washed with distilled water again.

1.3 Fabrication of various three-dimensional architectures

Hydrothermal process was conducted in sealed containers for the synthesis of CeO_2 and $FeOOH$ and in 45 mL hydrothermal reactors for the synthesis of other materials. The modified substrates with suitable size (depending on the size of container) were put into the growth solution (the contents were listed in Table S1). Then the hydrothermal process was conducted

in air dry ovens. When the reactions finished, substrates were washed carefully with water and then washed in sonic bath for 10 s to clean deposited impurities on substrates (BFWs cannot be washed in sonic bath, because their scales will peel off under that condition). All products were dried under room temperature.

Table S1 Hydrothermal synthetic condition for fabricating 3D architecture nanomaterials on substrates.

Materials	Growth solutions	Hydrothermal period (h)	Hydrothermal temperature (°C)
CeO ₂	Cerium (III) nitrate hexahydrate (0.1 g), urea (0.1 g), deionized water (20 mL)	4–6	80
Ni(OH) ₂	Nickel nitrate (0.1 g), urea (0.1 g), deionized water (20 mL)	9–12	110
WO ₃ ^[1]	Pluronic P123 (0.2g), ethyl alcohol (13 mL), tungsten (VI) chloride (0.2–0.4)	2	110
FeOOH	Ferric nitrate (0.1 g), urea (0.1 g), deionized water (20 mL)	4–5	80

1.4 Material characterizations

The X-ray diffraction (XRD) analysis was conducted with a D-max/2550 diffractometer (nickel filtered Cu α radiation, $\lambda=0.15406$ nm, 35 kV, 20 mA, sweeping speed: 4° min⁻¹). Inductively coupled plasma optical emission spectroscopy (ICP-OES) data was recorded with an Agilent ICP-OES 730 system. Transmission electron microscope (TEM) analyses were performed on a Talos F200X transmission electron microscope (200 kV, FEI, America). Scanning electron microscope (SEM) studies were carried out on JSM-7800F Prime scanning electron microscope (5 kV for morphology observation and 10 kV for EDS mapping, JEOL,

Japan) equipped with an energy dispersive spectrometer (NORANTM System 7, Thermo Scientific, US) and another Mira3 scanning electron microscope (5 kV for morphology observation, Tescan, Czech). Infrared (IR) and Raman spectra were measured using a Thermo Fisher Nicolet 6700 system and a dispersive Raman microscope (Senterra R200-L, Bruker, Germany), respectively. X-ray photoelectron spectroscopy (XPS) was conducted on spectroscope (AXIS-Ultra DLD, Shimadzu, Japan) to collect data.

1.5 Electrochemical test

Resistivity measurement: The samples were cut into rectangle slices. Then their resistances were measured with electrochemical impedance spectroscopy (EIS) and four probe method. The resistivity calculation of the four probe method follows this equation: $\rho = R \cdot C \cdot G(W/s) \cdot D(d/s)$, and $C = 20\pi / (1/S_1 + 1/S_2 - 1/(S_1 + S_2) - 1/(S_2 + S_3))$.

Where ρ , R , W , s , and d denote resistivity, resistance, thickness, distance between probes, and distance from the edge of the sample to the nearest probe. S_1 , S_2 , and S_3 is the distance from probe 1 to probe 2, probe 2 to probe 3, and probe 3 to probe 4, respectively.

Calibration of reference electrodes: Calibration was performed with a reversible hydrogen electrode (RHE) prior to initial use. Two Pt electrodes were pretreated with aqua regia for 10 s and then cycled in 0.5 M H_2SO_4 ($\pm 2V$). These clean Pt electrodes and Hg/HgO electrode were used as working electrode, counter electrode, and reference electrode, respectively. To perform the calibration, hydrogen gas was injected into the electrolyte (1 M KOH) under vigorous stirring during the whole process. This three-electrode system was cycled ± 100 mV at a scan rate of 1 mV s^{-1} around the expected value for the RHE. The RHE potential was the average potential of the forward and reverse sweep at zero current.

Oxygen evolution reaction (OER) test Test: Oxygen evolution reaction (OER) tests were conducted in standard three electrodes system. FeOOH–NF, Pt electrode, and Hg/HgO electrode were used as working electrode, counter electrode, and referee electrode, respectively. 1.0 M KOH solution was used as the electrolyte for all the electrochemical measurements. In a typical test, high purity oxygen (99.999%) was bubbled into the electrolyte for 30 min before electrochemical processes. The working electrode was assembled by gold electrode holder and FeOOH–NF (geometric area: 0.25–0.35 cm², following the equation: length×wide). A chronopotentiometry test was conducted as a pretreatment process until the overpotential of the working electrode tends to be stable (running for ca. 5 min). Linear sweep voltammetry (LSV) was carried out at 5.0 mV s⁻¹ for the polarization curves and at 0.1 mV s⁻¹ for the Tafel slope calculation. The uncompensated resistance of the cell was measured with a single-point high-frequency impedance measurement (100 kHz with 20 mV amplitude at the open-circuit potential), and IR drop was compensated at 85 % using the EC-Lab software. The chronopotentiometry tests were recorded without IR drops correction. EIS measurements were performed at 0.3 V (vs. Hg/HgO referee electrode) with 10 mV amplitude and frequencies ranging from 200 kHz to 10 mHz.

2. Mechanism analysis of Ce⁴⁺ modification process

2.1 Characterization of modification process on other substrates

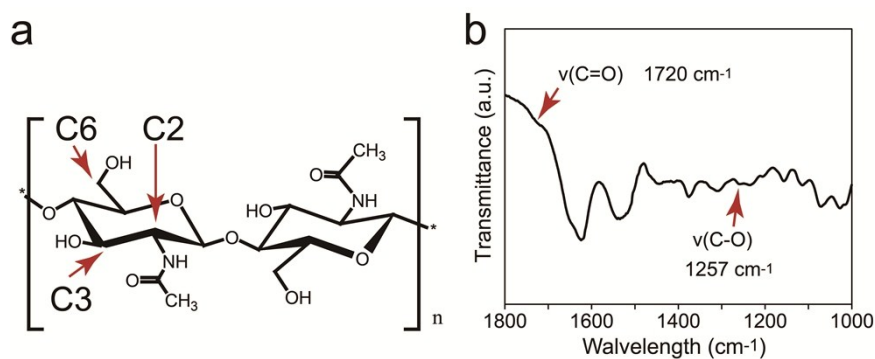


Fig. S1 (a) Chemical structure of chitin (main content of butterfly wings); (b) IR spectrum of Ce-BFWs immersed in 0.1 M HCl for 5 min. The $\nu(\text{C}=\text{O})$ and $\nu(\text{C}-\text{O})$ of COOH appeared after treating Ce-BFWs (include COO^-) with acid solution.

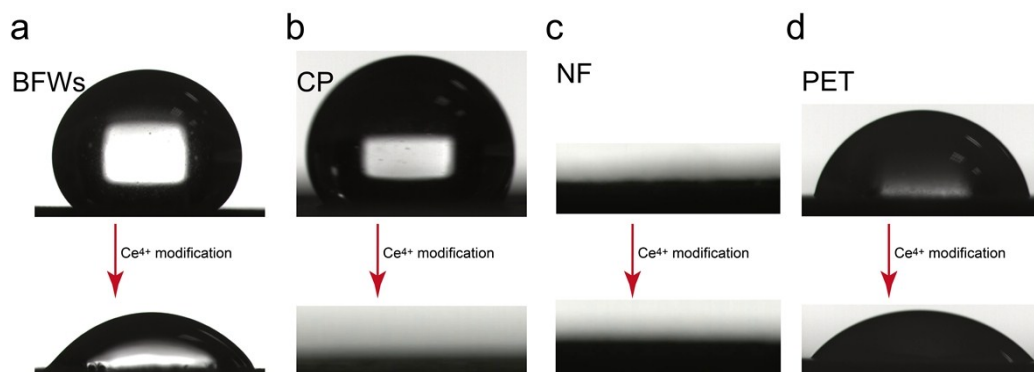


Fig. S2 Contact angles before and after Ce^{4+} modification process. (a) BFWs, (b) CP; (c) NF; (d) PET.

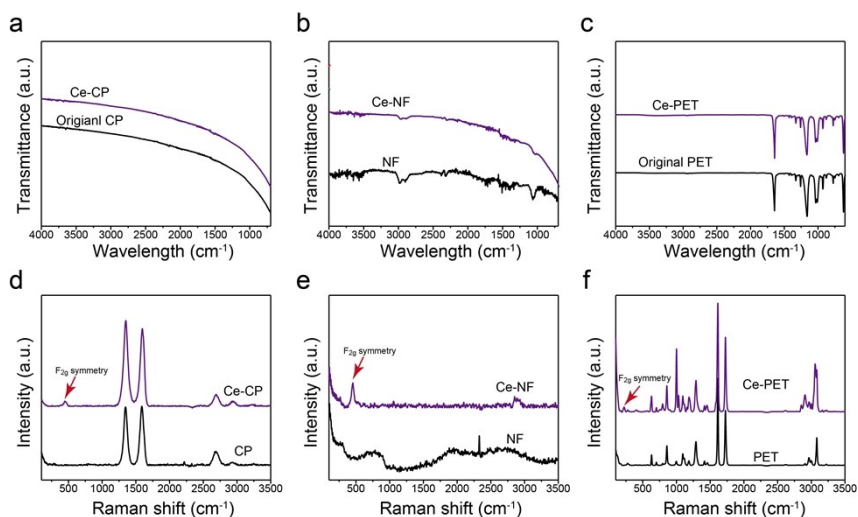


Fig. S3 IR and Raman spectra of original and Ce^{4+} modified substrates. (a), (d) CP; (b), (e) NF; (c), (f) PET.

2.2 Morphology characterization of Ce-BFWs

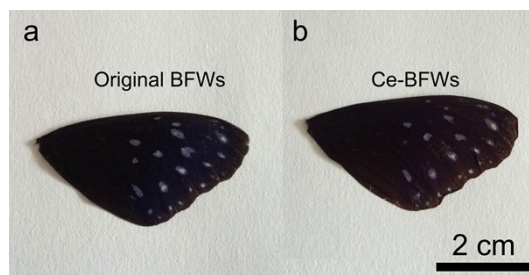


Fig. S4 Optical images of (a) original BFWs; (b) BFWs modified with Ce^{4+} for 15 min.

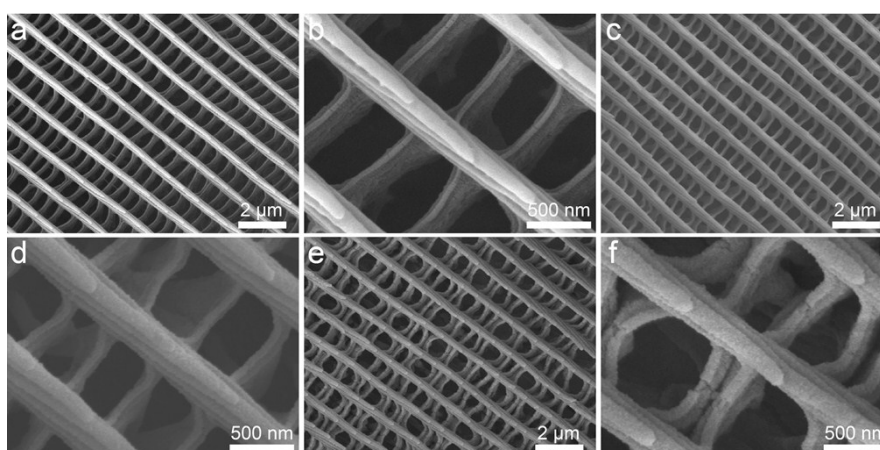


Fig. S5 Influence of modification time on the morphology of BFWs. (a), (b) Original BFWs; (c), (d) BFWs modified with Ce^{4+} for 5 min; (e), (f) BFWs modified with Ce^{4+} for 15 min.

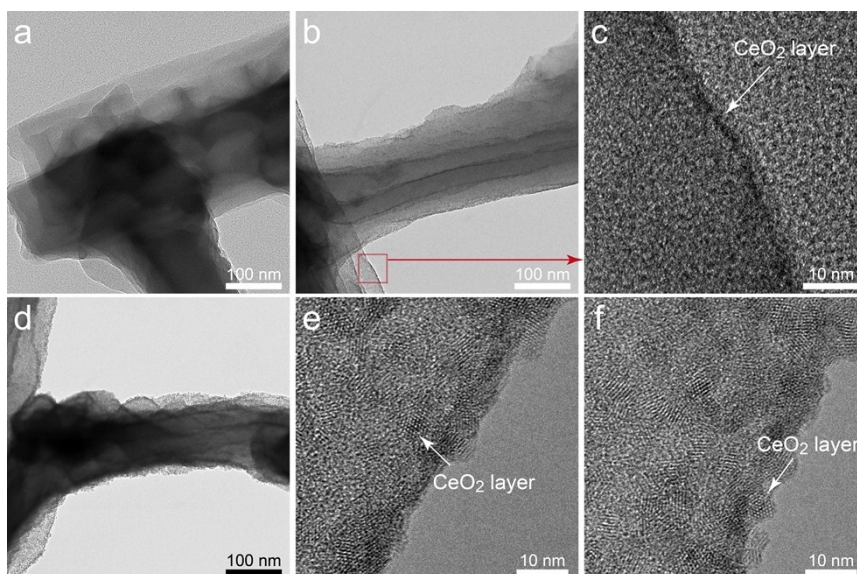


Fig. S6 TEM images of (a) original BFWs; (b) BFWs modified with Ce^{4+} for 5 min; (c) High-resolution TEM (HRTEM) of (b); (d) BFWs modified with Ce^{4+} for 15min and (e), (f) HRTEM of (d). Coverage percent of CeO_2 seeds on the surface of BFWs is calculated by the average results of (e) and (f).

2.3 Morphology characterization of other modified substrates

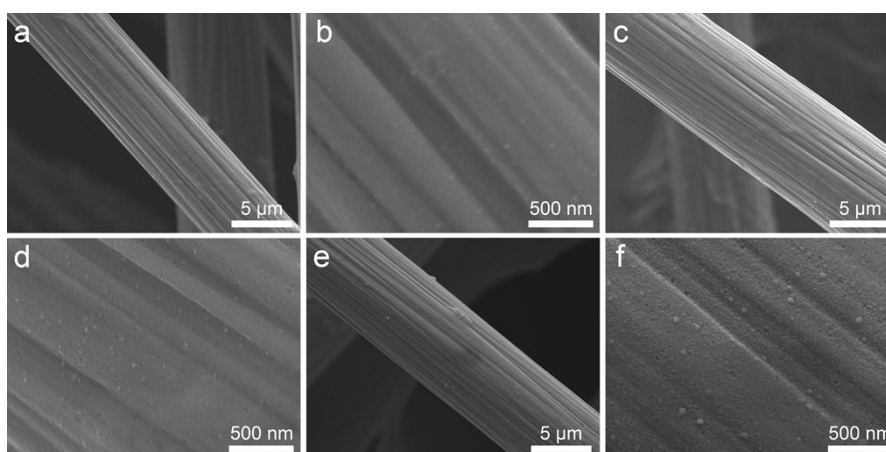


Fig. S7 Influence of Ce^{4+} modification time on CP. (a), (b) Original CP; (c), (d) CP modified with Ce^{4+} for 5 min; (e), (f) CP modified with Ce^{4+} for 2h.

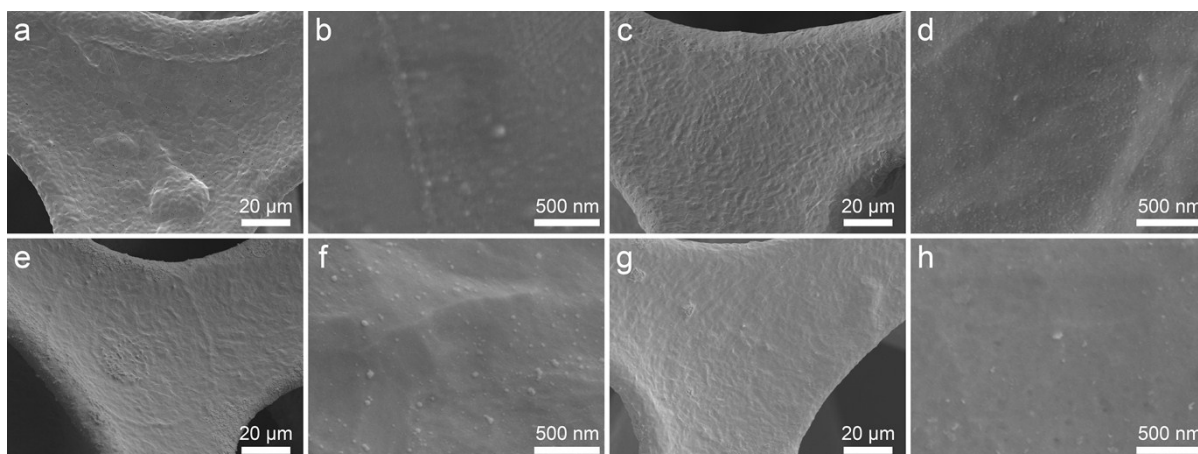


Fig. S8 Influence of Ce^{4+} modification time on NF. (a), (b) Original NF; (c), (d) NF modified with Ce^{4+} for 10 min; (e), (f) NF modified with Ce^{4+} for 15 min; (g), (h) NF modified with Ce^{4+} for 25 min.

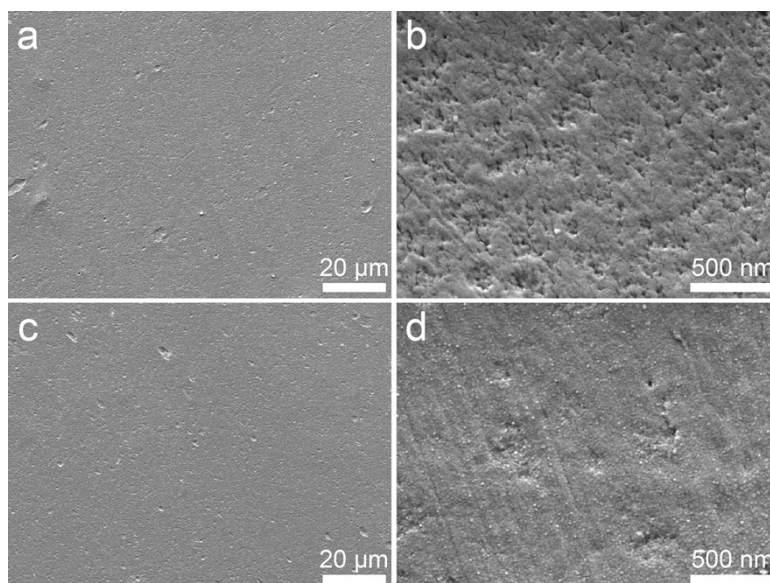


Fig. S9 Influence of Ce^{4+} modification process. (a), (b) Morphology of original PET; (c), (d) Morphology of PET immersed in Ce^{4+} solution for 2 h.

Contact angle measurement, IR and Raman tests were conducted on CP, NF, and PET to study their modification mechanism. All three substrates show hydrophilic surfaces after Ce^{4+} modification process (Fig. S2), indicating that surface functional groups changed during the

modification process. Though their IR spectra (Fig. S3a-c) have no obvious peak changes, their Raman spectra all show the newborn peak at 455 cm^{-1} (Fig. S3d-f). These results indicate the generation of CeO_2 nanoparticles on the surface of these substrates. Meanwhile, the SEM images of the original and modified substrates show that the original structure of these substrates were maintained after the modification process (Fig. S7-9). So the change of functional groups and the formation of CeO_2 seeds both happened on the surface of CP, NF and PET, though the changes of functional groups are different among these substrates.

3. Mechanism analysis of growing three-dimensional architectures on substrates

3.1 Mechanism analysis of growing CeO_2 on H_2O_2 and HNO_3 modified BFWs

Table S2 ICP-OES results of CeO_2 growth process on Ce-BFWs. These processes were recorded every one hour.

Time	0 h	1 h	2 h	3 h	4 h
Ce (wt.%)	1.13	2.45	6.14	11.24	19.83
Variation	/	1.13	3.69	5.10	8.59

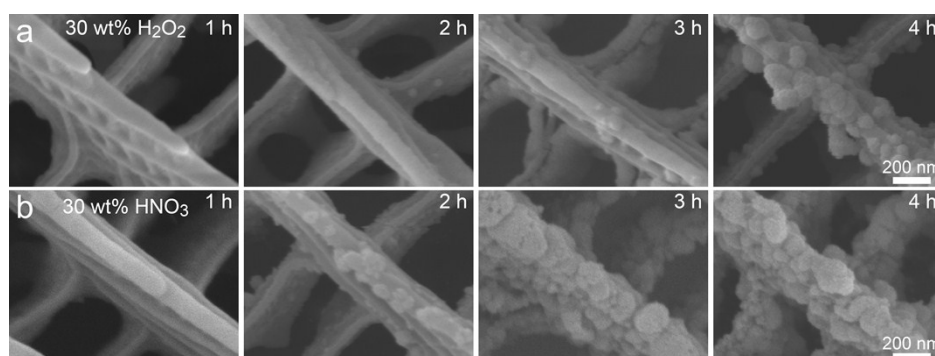


Fig. S10 SEM images of CeO_2 growth process on (a) 30 wt.% H_2O_2 modified BFWs (b) 30 wt.% HNO_3 modified BFWs. These processes were recorded every one hour. 30 wt.% HNO_3 and 30 wt.% H_2O_2 can introduce functional groups on BFWs in a similar way as Ce^{4+} ions (oxidizing process) without generating CeO_2 seeds.

3.2 Mechanism analysis of growing FeOOH on modified nickel foam

Growth process of FeOOH on Ce⁴⁺ modified NF (Fig. S11) shows that the size of FeOOH on the surface of NF is pretty small at the first hour. Then the FeOOH grew larger and covered the whole surface of NF. Finally, an intact FeOOH layer composing of sheets larger than 200 nm formed on the surface of NF.

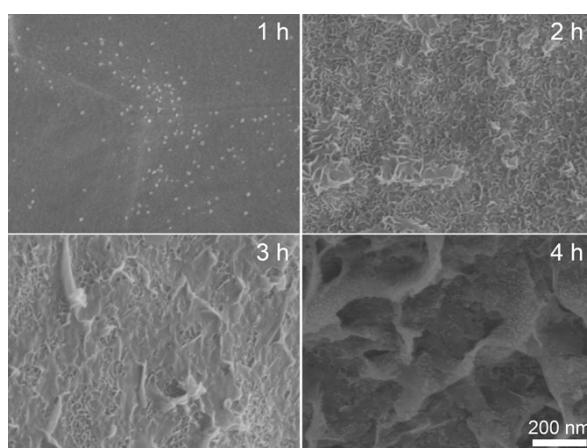


Fig. S11 SEM images of growing FeOOH on Ce⁴⁺ modified NF, this process was recorded every one hour.

4. Morphology of three-dimensional architectures fabricated on unmodified and modified substrates

4.1 Morphology of CeO₂ grown on unmodified substrates

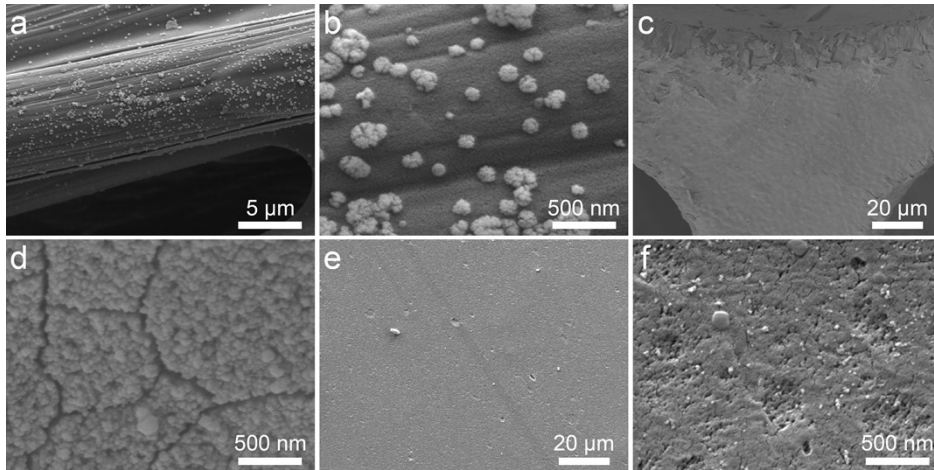


Fig. S12 SEM images of CeO₂ fabricated on unmodified substrates. (a), (b) CP. (c), (d) NF. (e), (f) PET.

4.2 Morphology of other 3D architecture fabricated on modified substrates

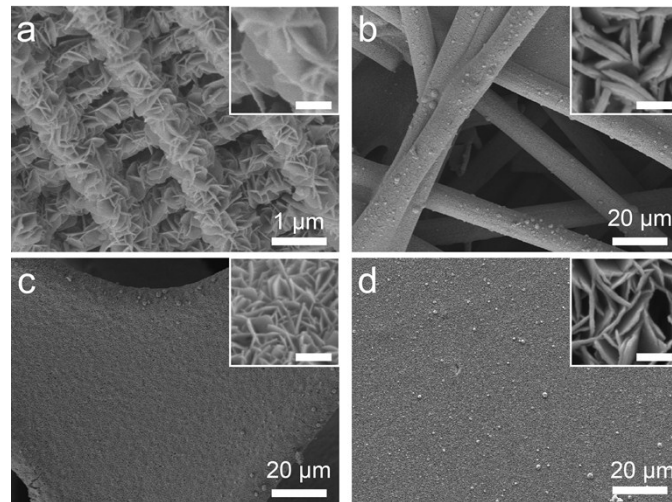


Fig. S13 Morphology of WO₃ nanosheets fabricated on (a) BFWs; (b) CPs; (c) NF; (d) PET. The insets show the corresponding high multiple SEM images with scale bar of 250 nm.

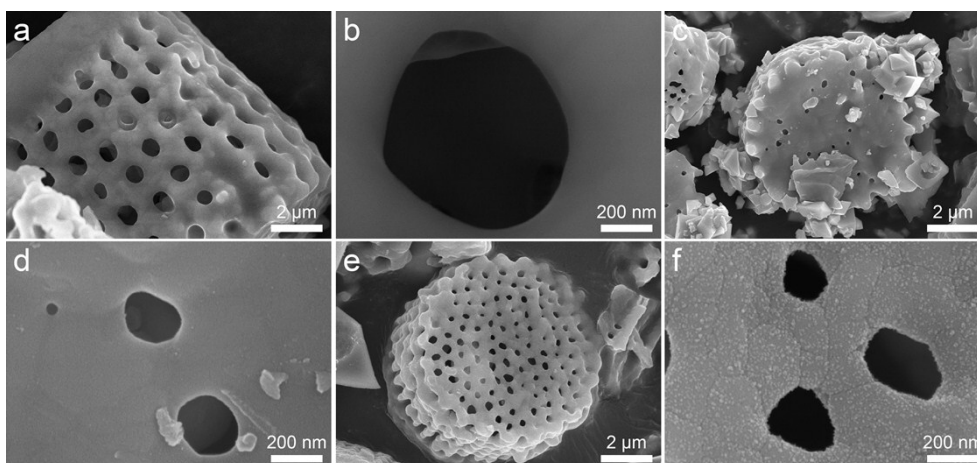


Fig. S14 SEM images of (a), (b) Original diatomite; (c), (d) CeO_2 fabricated on unmodified diatomite; (e), (f) CeO_2 fabricated on Ce^{4+} modified diatomite.

4.3 The XRD patterns of the nanomaterials on substrates

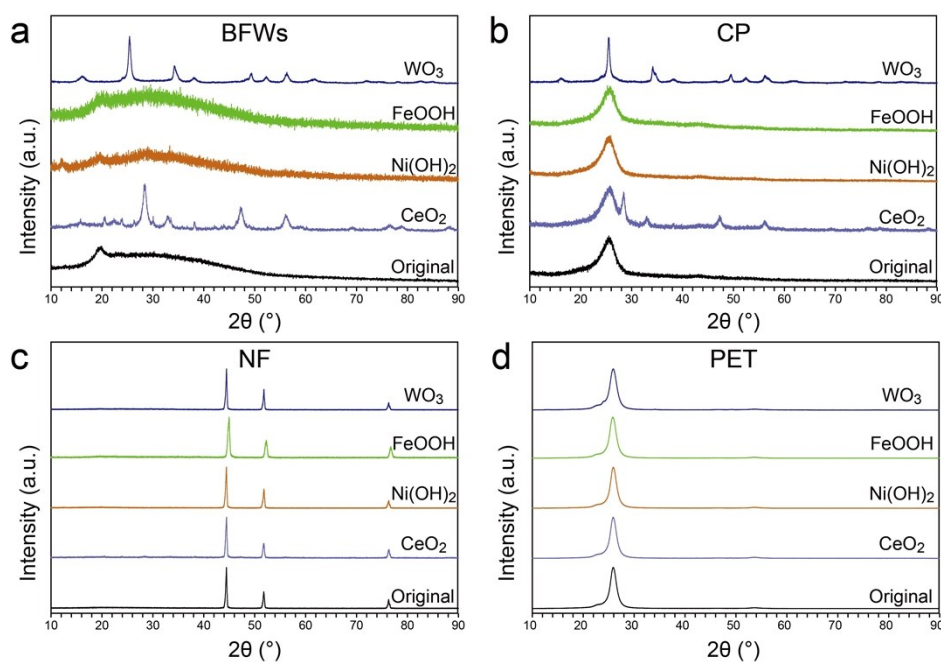


Fig. S15 XRD patterns of the nanomaterials fabricated on different substrates. (a) BFWs; (b) CP; (c) NF; (d) PET. These materials are CeO_2 (JCPDF No. 81-0792), Ni(OH)_2 (JCPDF No. 22-0444), FeOOH (JCPDF No. 44-1415), and WO_3 (JCPDF No. 84-0886). When these

nanomaterials were fabricated on CP, NF, and PET, strong diffraction peaks of substrates make them difficult to discern the diffraction peaks of the fabricated nanomaterials.

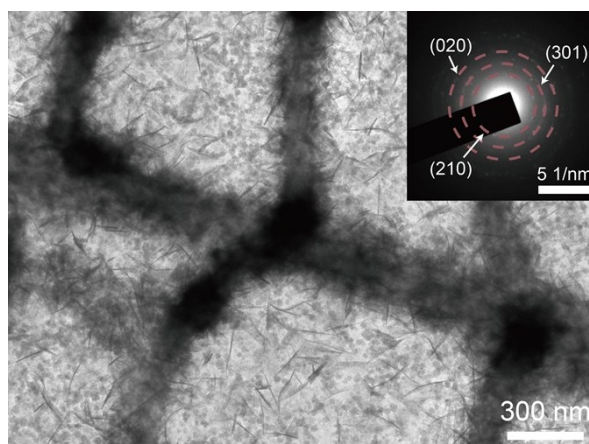


Fig. S16 TEM image of FeOOH on Ce-BFWs. The inset is a corresponding selected area electron diffraction pattern. These results are utilized to assist the composition analysis of the FeOOH on Ce-BFWs.

5. Electro catalysis performance

5.1 Standardization of Hg/HgO referee electrode

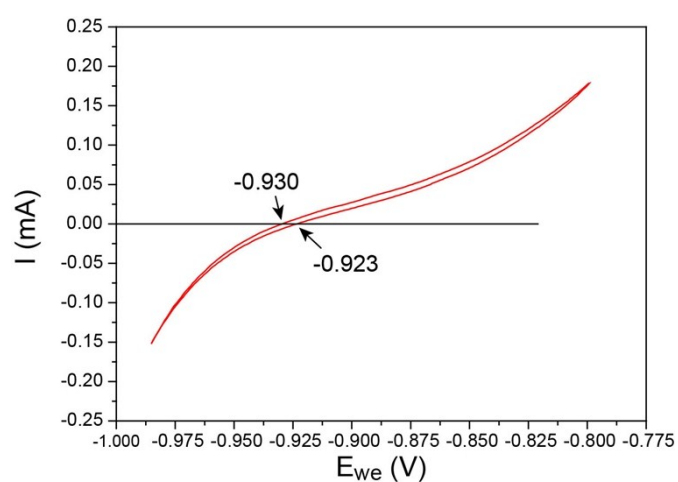


Fig. S17 CV curve of Hg/HgO referee electrode. RHE potential in our system was -0.926 V vs. Hg/HgO referee electrode.

5.2 Resistivity calculation of modified and unmodified nickel foam

For EIS method, resistivity was calculated following the equation: $\rho=RS/L$. The resistivities of HCl–NF and Ce–NF are $1.34\times 10^{-5} \Omega \text{ m}$ and $4.65\times 10^{-5} \Omega \text{ m}$, respectively. For four probe method, the resistances of HCl–NF and Ce–NF were $2.48\times 10^{-3} \Omega$ and $6.68\times 10^{-3} \Omega$. There, $G(\text{HCl–NF})=0.8158$; $G(\text{Ce–NF})=0.8132$; D is 0.5958. So the resistivities of HCl–NF, Ce–NF are $7.5\times 10^{-5} \Omega \text{ m}$, $2.031\times 10^{-4} \Omega \text{ m}$, respectively.

The resistivity from four probe method is higher than that from EIS method, which can be attributed to conductive binders (silver paste) utilized in the four-probe method. But their tendencies are similar: the resistivity of substrates increases after Ce^{4+} modification, but remains in the same order of magnitude of the original substrates.

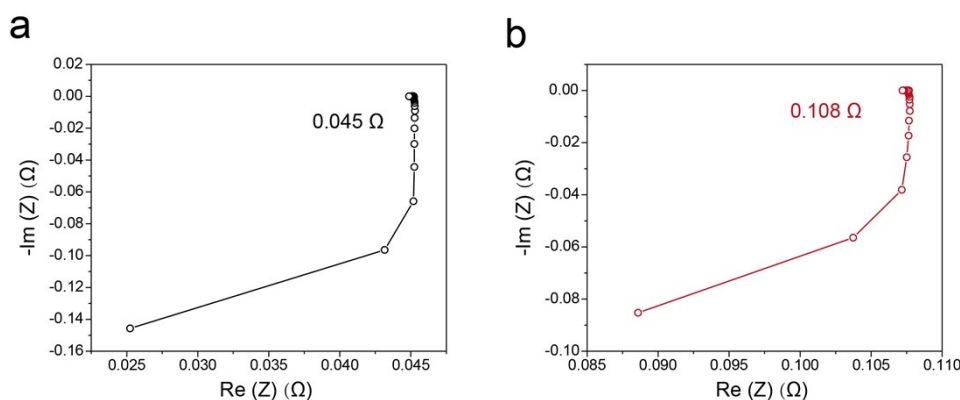


Fig. S18 EIS spectrum of (a) HCl pretreated NF (HCl–NF, length: 15 mm; width: 3 mm; thickness: 1.487 mm) (b) Ce⁴⁺ modified NF (Ce–NF length: 13 mm; width: 4 mm; thickness: 1.40 mm).

5.3 Electrocatalysis performance of original nickel foam

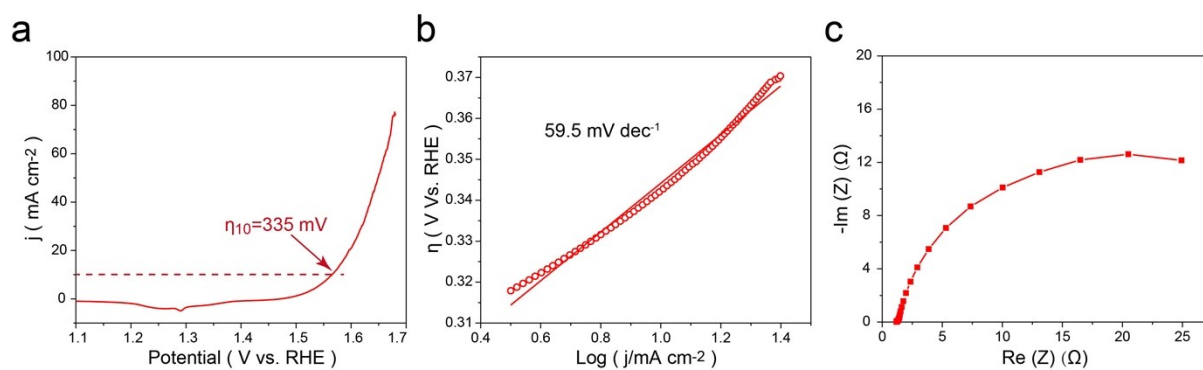


Fig. S19 (a) IR-corrected (85 % IR drop compensation) OER LSV curve; (b) Corresponding Tafel plot; (c) EIS of HCl-NF.

5.4 Morphology comparison of FeOOH on nickel foam

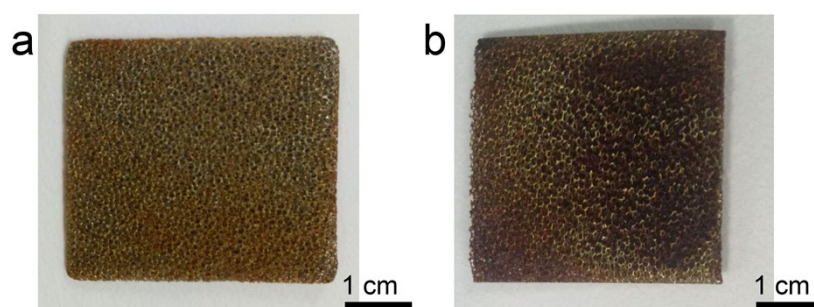


Fig. S20 Photo images of FeOOH grown on (a) Ce^{4+} ions modified NF and (b) HCl-NF. Compared with FeOOH on HCl-NF, the FeOOH on Ce^{4+} modified NF shows a uniform large-area coating of FeOOH

Notes and references

- 1 Sun, Z.; Liao, T.; Dou, Y.; Hwang, S. M.; Park, M.-S.; Jiang, L.; Kim, J. H.; Dou, S. X, Nat. Commun. **2014**, 5, 3813.